DETECTION OF BARCHAN DUNES IN HIGH RESOLUTION SATELLITE IMAGES

M. A. Azzaoui [a,*], M. Adnani [a], H. El Belrhiti [b], I. E. Chaouki [c], C. Masmoudi [a]

[a] Laboratoire d'Electronique et de Traitement du Signal/ Géomatique (LETS/Géomat Faculté
des Sciences de Rabat, Université Mohammed V-Agdal, 4 Avenue Ibn Battouta B.P. 1014
RP, Rabat, Maroc. - azzaoui.m.amine@gmail.com, adnani.manar@gmail.com,
lhmasmoudi@gmail.com

[b] Département des Sciences Fondamentales et Appliquées. Institut Agronomique et
Vétérinaire Hassan II. BP 6202, 10101 – Rabat, Maroc - helbelrhiti@gmail.com or
h.elbelrhiti@iav.ac.ma

[c] Ecole Nationale des Sciences Appliquées d'Agadir, Maroc. B.P. 1136. -
b.chaouki@uiz.ac.ma

WG VII/4 - Methods for Image Classification – Full Papers

ABSTRACT:

Barchan dunes are the fastest moving sand dunes in the desert. We developed a process to detect barchans dunes on High resolution satellite images. It consisted of three steps, we first enhanced the image using histogram equalization and noise reduction filters. Then, the second step proceeds to eliminate the parts of the image having a texture different from that of the barchans dunes. Using supervised learning, we tested a coarse to fine textural analysis based on Kolomogorov Smirnov test and Youden's J-statistic on co-occurrence matrix. As an output we obtained a mask that we used in the next step to reduce the search area. In the third step we used a gliding window on the mask and check SURF features with SVM to get barchans dunes candidates. Detected barchans dunes were considered as the fusion of overlapping candidates. The results of this approach were very satisfying in processing time and precision.

1. INTRODUCTION

1.1 Barchan dunes

Barchans are one type of sand dunes. They were differentiated from other sand dunes using several criteria. While Star Dunes were formed in wind regime with high directional variability and Linear Seif Dunes were formed under bidirectional wind regimes beating the dune obliquely, Barchan dunes were formed under a unidirectional-wind mechanism (Tsoar, 2001). We also highlighted that a distinction should be made between simple, compound and complex sand dunes. Dunes that were spatially separated from other nearby dunes were considered simple. When two or more dunes of the same type coalesced or superimposed, they were considered as compound. And if dunes from different types coalesced or superimposed, they were considered as complex (McKee, 1979). Barchans were defined as isolated crescent-shaped mobile dunes which had insufficient sediment supply to cover the entire substratum. The horns of a barchan pointed in the direction of dune movement. They might be scattered over bare rock surfaces. Barchans possessed a windward convex side and a steeper lee side with two horns that faced downwind and a slip face. (Elbelrhiti and Hargitai, 2015). Barchans could be subaqueous or Aeolian (Hersen, 2005). They were known to be found on Earth, but were also an extra-terrestrial phenomenon. Indeed, Barchan dunes were found in Mars, Venus and Titan (Bourke et al., 2010).

On one hand, the study of Barchan dunes played important role in the context of natural hazard monitoring, mapping and management. The fact that Barchan dunes were the fastest sand dunes made of them a threat for many human activities, mainly in arid or semi-arid areas. On the other hand, the study of Barchan dunes or Barchans dunes fields was important in the exploration of other planetary landforms. The orientation of Barchans that were found in Mars was used to infer near-surface wind regimes (Bourke, 2010). While active sand dunes would reflect present-day prevailing winds, the dormant sand dunes would record wind patterns from older wind regimes that were now defunct (Fenton 2006). Studies were also concerned about understanding the spatial patterns occurring in dune fields (Bishop, 2007; Bourke et al. 2008; Silvestro et al., 2010).

1.2 Remote sensing

Remote sensing imagery played an important role in the analysis of barchans dunes fields. The use of remote sensing was useful since the first studies which were concerned about the mapping and the taxonomy of sand dunes (McKee, 1979). Later, remote sensing helped researchers to find a correlation between the types of sand dunes and the vegetation cover, the wind direction and the availability of sand (Wasson and Hyde, 1983; Fryberger, 1979). More recently, with the developments of remote sensing, the attention of researchers was drawn from the study of individual dunes, that constituted the bulk of literature (Livingstone et al., 2007), to the large-scale study of dune fields, by using spatial analysis and investigating inter-dunes relations, dune-field patterns and hierarchies (Tsoar and

---

* Corresponding author

Blumberg, 2002; Kocurek and Ewing, 2005; Hugenholtz and Wolfe, 2005a; Mitasova et al., 2005; Ewing et al., 2006; Bishop, 2007; Wilkins and Ford, 2007; Ewing and Kocurek, 2010a, b; Hugenholtz and Barchyn, 2010; Kocurek et al., 2010; Hugenholtz et al. 2012). For planetary landforms such as Mars, they were essential in the study of Barchans. Since 1964, five major imaging programs revealed that dunes were widespread in Mars (Mariner 9; Viking; Mars Global Surveyor, MGS; Mars Odyssey; and Mars Reconnaissance Orbiter, MRO) (Hugenholtz et al. 2012). Barchan dunes were generally scattered and were often distinguished by their spatial properties, in addition to their spectral properties (Blanco et al., 2007). Pixel based methods were used for mapping Barchan dunes. The classifications were based on the application of Parallelepiped, Minimum Distance and Maximum Likelihood techniques (Richards and Jia, 2006). Nevertheless, good results were obtained with object-oriented approaches (Wilkinson, 1999). In fact, in the case of remote sensing, the use of segmentation methods (Pal and Pal, 1993) increased progressively and replaced the use of pixel-based methods (Blaschke and Strobl 2001, Blaschke et al. 2004), while their use in other areas such as pedestrian recognition (Benenson et al., 2014), or medical analysis (Sivaramakrishnan et al. 2014) were legion. The actual object based image analysis (OBIA) or geospatial object based image analysis (GEOBIA) were also gaining an important share of literature (Blaschke 2010), and they were converging towards mainstream GIS applications (Baatz et al., 2008). Image processing approaches could achieve object detection and recognition through the use of object models based on shape, motion, color or texture (Jain and Chadokar, 2015). The use of adequate features and features engineering was important along with the use of adapted classifiers to accomplish good results. Among the most cited feature extraction methods, many descriptors and detectors were available, such as Harris, Binary Robust Invariant Scalable Keypoints (BRISK), Fast Retina Keypoint (FREAK), Binary Robust Independent Elementary Features (BRIEF), Oriented FAST and Rotated BRIEF (ORB), Maximally Stable Extremal Regions (MSER) detectors. Other features such as Haralick, Local Binary Patterns (LBP) and Histogram of Oriented Gradients (HOG) served as descriptors. While Scale-Invariant Feature Transform (SIFT) and Speed-Up Robust Features (SURF) could be used as detectors and descriptors. For the classification or regression techniques, Logistic regression (LR), Support Vector Machines (SVM) and artificial neural networks (ANN), deep learning (DL) and their variations could be used. Also, Markov Random Field (MRV) was a popular technique among researchers for the classification of remote sensing images (Li et al. 2014).

2. MATERIAL AND METHODS

2.1 Material

The satellite image we used was taken by the High Resolution Imaging Science Experiment (HiRISE) instrument mounted on the Mars Reconnaissance Orbiter. The "ESP_034815_2035" image provided by NASA/JPL/University of Arizona contained a Barchans field with a formation of 60 Barchan dunes. This field was located in a crater near Mawrth Vallis, which was presented as a possible landing site for Mars 2020 (Loizeau et al. 2015). The following table contained the details about this image [Table.1].

Planet	Mars
Satellite	Mars Reconnaissance Orbiter, MRO
Location	A large crater near Mawrth Vallis, Oxia Palus Quadrangle
Coordinates	Maximum latitude = 23.292862° Minimum latitude = 23.088633° Eastern Most longitude=339.650653° Western Most longitude = 339.529501°
Scale	0.25 meters/pixel
Date	December 30th, 2013
Area	32.38 km²

Table 1. Details about the image used

2.2 Methods

2.2.1 Overall architecture: A Machine Learning approach was used, as we divided the image into small tiles that were separated in three groups: the learning set, the validation set and the test set. The methods that were described in the following sub-chapters required setting their respective parameters values, and assessing their generalization capability. This was done using cross validation. Also, two sliding window scales were evaluated: the 128x128 and 64x64. Once the learning stage was finished, we proceeded to the test stage, which started with image enhancement, then texture analysis, then the selection of candidates [Alg.1], and finally the fusion of candidates.

```
For Each MSER region
    score ← 0
    region_surf_counter ← 0
    region_positive_surf_counter ← 0
    For Each SURF point
        If SURF point inside MSER region
            INCREMENT region_surf_counter

            If svm.predict(SURF) = = 1
                INCREMENT region_positive_surf_counter
            End
        End
        score ← region_positive_surf_counter / region_surf_counter
        If score > 50%
            BB ← min_Bounding_Box(MSER region)

            List_candidates.add(BB)
        End
    End
End
```

Alg.1 Pseudo algorithm of candidates selection

To go through the [Alg.1], the tiles (image samples) had first to be evaluated as positives, by a prior texture analysis. This first step was achieved using Haralick features of a GLCM. The features thresholds were set using Youden's statistic. Thus, if the image was declared negative by the texture analysis, no further processing was executed. Of course, a high false positives rate was adopted to skip no dune, while reducing consequently the search space. The idea behind the second step [Alg.1] was to extract MSER regions that were used to eliminate unwanted SURF points (which happened to be outside all MSER regions), then conversely, these same SURF points scored the MSER region they belonged to (and eliminated the MSER regions with no SURF points). The score of a MSER region consisted of the ratio between the positive SURF points on the total number of SURF points. This meant that MSER regions having a low number of positive SURF points relatively to negative ones were eliminated. The

remaining MSER regions were enclosed using minimal bounding box algorithm and qualified as candidates for the next step. This final step consisted of merging overlapping bounding boxes into positive detections of barchans dunes. The same process was executed using a 64x64 sliding window and the results were compared.

2.2.2   Image pre-processing: The contrast of image was adjusted so that 1% of pixels were saturated at low and high intensities. Then, two 2-D adaptative noise removal filters were applied: The first was Wiener filter which was based on the mean and variance estimations from a local neighbourhood of each anchor pixel. The second filter that was applied was the median filter with a 3x3 window.

2.2.3   Grey-Level Co-occurrence Matrix and Haralick Features: The image was cut-out into sample images for which the GLCM and Haralick features were extracted. The GLCM was used after reducing image samples grey levels to 16 in order to improve time efficiency without losing much information. The GLCM was extracted along the 4 directions (0°, 45°, 90° and 135°), and the offset chosen was the first pixel neighbour. Then the following Haralick features were extracted: The Autocorrelation, Contrast, Correlation, Cluster Prominence, Cluster Shade, Dissimilarity, Energy, Entropy, Homogeneity, Maximum probability, Sum of squares Variance, Sum average, Sum variance, Sum entropy, Difference variance, Difference entropy, Information measure of correlation, Inverse difference normalized and Inverse difference moment normalized (Soh, 1999; Haralick, 1973; Clausi 2002).

2.2.4   Kolmogorov–Smirnov test and Youden's J statistic: The sample images from the training set were labelled as positives or negatives. The Two-sample Kolmogorov–Smirnov test was then used to measure the distance between probability distributions of the positive and negative classes regarding each Haralick feature. The Haralick feature that scored the maximum distance was then chosen as the only parameter to classify positive and negative samples. We could use another approach that was based on boosting, by establishing a vote to develop a stronger classifier. But, we preferred choosing one parameter to reduce the execution time of the overall detection process. A threshold was calculated for the selected feature using Youden's J statistic which was used to find the optimum cut-off point that maximized the distance between the Receiver Operating Curve (ROC) and the Chance level line. A binary sign was also calculated and saved. When this sign equalled 1, it meant that the positives are superior to the threshold value, and when it was equal to -1, it meant that the positives were inferior to the threshold value.

2.2.5   Speed-Up Robust Features and Maximally Stable Extremal Regions: Speed-Up Robust Features, SURF (Leibe et al. 2008) were used as feature detectors and descriptors. They were extracted for all the test sample images using the scales used. The SURF-128 was used instead of SURF-64 in order to improve the accuracy of the results. In the training stage, the points were labelled as positive or negative depending on their proximity to the barchans dunes. The SURF points were selected when the stronger feature threshold was above 30 to ensure that sufficient positive feature points were detected. In fact, the SURF negative points were way more numerous than positive points, due to the sparse Barchan dunes positions. In order to balance our training set, we selected an equal number of positive and negative SURF points, with of course, a random selection of the negative SURF to ensure a limited bias. Following, we clustered the negative SURF points using K-Means. We could choose K as equal to the number of positive points. However, the results using random selection were satisfactory, and moreover, the use of a clustering algorithm would have affect the execution time of the learning phase.
The Maximally Stable Extremal Regions MSER (Matas et al. 2002) detector was also used to detect blob regions. The parameters were adjusted on training samples. The Maximum area variation between extremal regions at varying intensity thresholds was chosen as 30%.

2.2.6   Support Vector Machines: The Support Vector Machines SVM (Cortes and Vapnik, 1995) was a classification technique which consisted to find a hyperplane separating two classes by maximizing the separation margin. It was based on the decision function:

$$f(\mathbf{x}) = sign\left(\sum_{x_i \in S}^{n} (y_i \alpha_i K(x_i, \mathbf{x}) + b)\right) \quad (1)$$

We used a linear kernel SVM to classify the SURF features. SVM models were used for both scales used and the results were validated using cross-validation.

2.2.7   Bounding box fusion: The candidates were framed using minimum bounding box algorithm, which was based on convex hull. When the overlapping of candidates was above a threshold, the fusion of candidates resulted into a detection of a Barchan dune.

3.   RESULTS

The selected Haralick features for 128 and 64 sliding window sizes were respectively Cluster Prominence and Correlation. The following histograms showed the distribution of positive and negative samples for the 128 and 64 selected features [Figure.1] and [Figure.2].
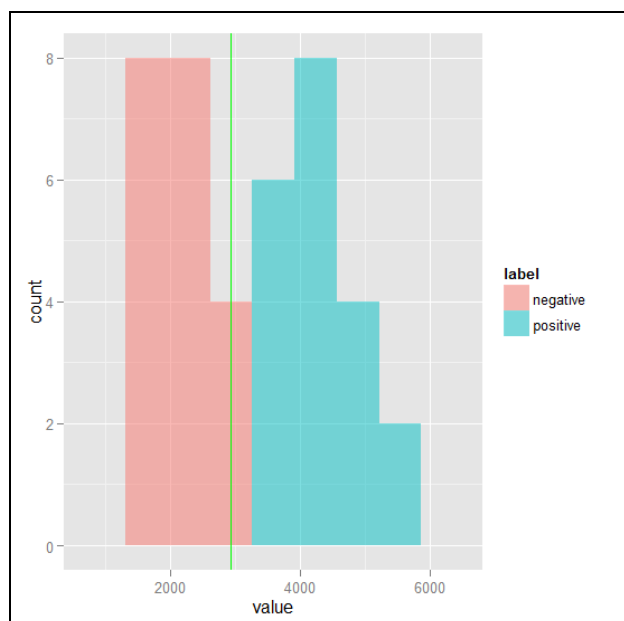
Figure 1. The separation with the green line (J statistic) between positive and negative features for the 128 scale
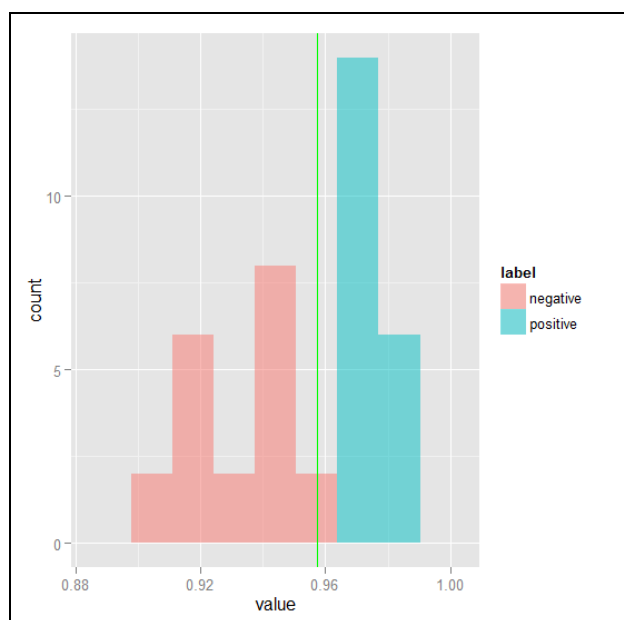

Figure 2. The separation with the green line (J statistic) between positive and negative features for the 64 scale

The SVM was learning was validated using 10 folds cross-validation on the learning set. The following table showed the error and execution times for each scale.

SURF-128	K-Fold (K=10) error	Learning execution time (s)	Testing execution time (s)
128 scale	0.0602	1.468286	27.232531
64 scale	0.0919	0.958666	19.767895

Table 1. SURF error and execution times

4. CONCLUSION

We experimented a method for detecting barchans dunes in high resolution satellite images. It consisted on several steps: Image enhancement, textural analysis with Kolomogorov Smirnov test and Youden's J-statistic on co-occurrence matrix Haralick features, then candidate selection and fusion using MSER regions and SVM classifier with SURF features, and finally the fusion of overlapping candidates. The 64x64 sliding window showed a better processing time than 128x128 window by 27%, but K-fold error revealed that the 128x128 sliding error was 33% less than 64x64 sliding window. Both scales allowed all the barchan dunes to be detected successfully and overall the method was satisfying in both processing time and precision.
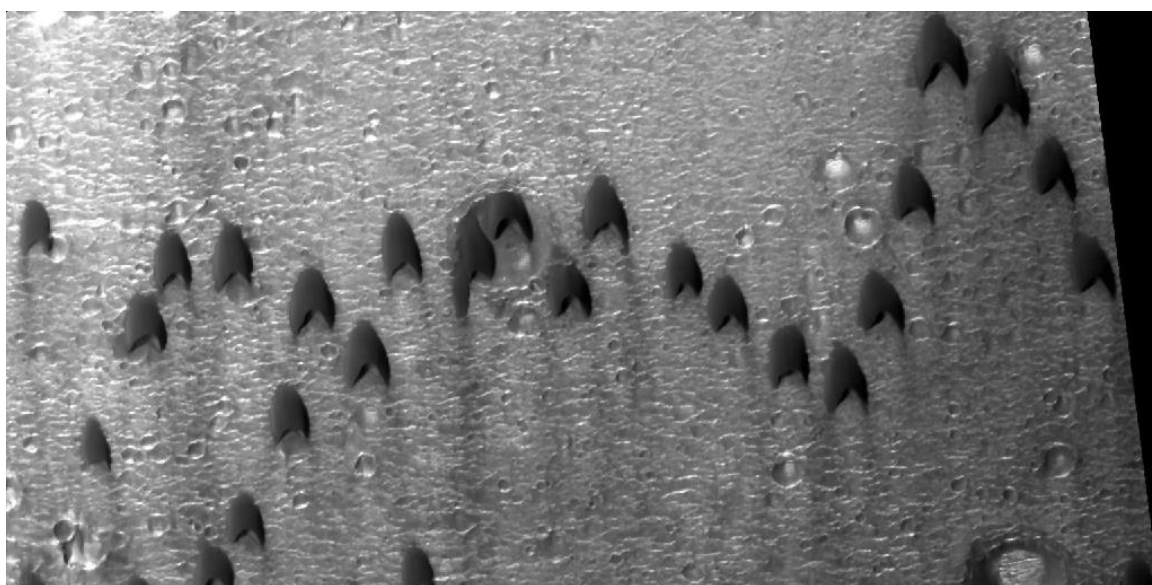
ACKNOWLEDGEMENTS (OPTIONAL)

REFERENCES

Baatz, M., Hoffmann, C., Willhauck, G., 2008. Progressing from object-based to object-oriented image analysis. In: Blaschke, T., Lang, S., Hay, G.J. (Eds.), Object based image analysis. Springer, Heidelberg, Berlin, New York, pp. 29_42.

Benenson R., Omran M., Hosang J., Schiele B.2014. Ten Years of Pedestrian Detection,What Have We Learned? Computer Vision - ECCV 2014 Workshops. Volume 8926 of the series Lecture Notes in Computer Science pp 613-627

Bishop, M.A., 2007. Point pattern analysis of North Polar crescentic dunes, Mars: A geography of dune self-organization. Icarus 191: 151-157.

Blanco, P.D., Graciela, M.H.F., and delValle, W., 2007, Assessment of Terra-ASTER and Radarsat imagery for discrimination of dunes in the Valdes Peninsula: an object-oriented approach. Revista de la Asociación Española de Teledetección, 28, 7–96.

Blaschke. T., 2010. Object based image analysis for remote sensing. ISPRS Journal of Photogrammetry and Remote Sensing. Volume 65, Issue 1, January 2010, Pages 2–16.

Blaschke. T., Strobl J. 2001. What's wrong with pixels? Some recent developments interfacing remote sensing and GIS.GIS– Zeitschrift für Geoinformations systeme, 14 (6) (2001), pp. 12–17

Blaschke T., Burnett C., Pekkarinen. A. 2004. New contextual approaches using image segmentation for object-based classification

Bourke M.C., Lancaster N., Fenton L.K., Parteli J.R.E., Zimbelman J.R., Radebaugh J. Extraterrestrial dunes: An introduction to the special issue on planetary dune systems. Geomorphology (2010) 1–14.

Bourke M.C., 2010, Barchan dune asymmetry: Observations from Mars and Earth. Icarus (2010) 183–197.

Bourke, M.C., Edgett, K.S., Cantor, B.A., 2008. Recent aeolian dune change on Mars, Geomorphology 94: 247-255.

Clausi D A., 2002. An analysis of co-occurrence texture statistics as a function of grey level quantization, Can. J. Remote Sensing, vol. 28, no.1, pp. 45-62, 2002.

Cortes, C.; Vapnik, V., 1995. "Support-vector networks". Machine Learning 20 (3): 273.

De Meer F., De Jong S. (Eds.), Remote Sensing Image Analysis: Including the spatial domain, Kluver Academic Publishers, Dordrecht (2004), pp. 211–236

Elbelrhiti, H. and Hargitai H: 2015. Encyclopedia of Planetary Landforms, Chapter: Barchan, p123, Springer New York.

Ewing, R.C., Kocurek, G., 2010a. Aeolian dune-field pattern boundary conditions. 967 Geomorphology 114: 175–187

Ewing, R.C., Kocurek, G., Lake, L.W., 2006. Pattern analysis of dune-field parameters. Earth Surf. Proc. Land. 31: 1176–1191.

Fenton, L. K., 2006. Dune migration and slip face advancement in the Rabe Crater dunefield, Mars. Geophys. Res. Lett.

Fryberger, S.G., 1979. Dune forms and wind regime. In: E.D. McKee, (Editor), A study of global sand seas. U.S. Geological Survey Professional Paper 1052, 137-169

Haralick, R. M Shanmugam K., and I. Dinstein, 1973. Textural Features of Image Classification, IEEE Transactions on Systems, Man and Cybernetics, vol. SMC-3, no. 6, Nov 1973.

Hersen. P. 2005. Flow effects on the morphology and dynamics of aeolian and subaqueous barchan dune. Journal Of Geophysical Research, VOL. 110, F04S07, 2005.

Hugenholtz CH, Levin N, Barchyn TE, Baddock M, 2012. Remote sensing and spatial analysis of aeolian sand dunes: a review and outlook. Earth-Science Reviews 111: 319-334

Hugenholtz, C.H., Barchyn, T.E., 2010. Spatial analysis of sand dunes with a new global topographic dataset: new approaches and opportunities. Earth Surf. Proc. Land. 35: 986- 992.

Hugenholtz. C.H, Noam Levinc, Thomas E. Barchyna, Matthew C. Baddockd, 2010. Remote sensing and spatial analysis of aeolian sand dunes: A review and outlook. Earth-Science Reviews. Volume 111, Issues 3–4, March 2012, 319–334.

Hugenholtz, C.H., Wolfe, S.A., 2005. Biogeomorphic model of dunefield activation and stabilization on the northern Great Plains. Geomorphology 70: 53-70.

Jain S., Chadokar S., 2015. A Object Detection in Image Processing: A Review. International Journal of Electrical, Electronics and Computer Engineering 4(2): 26-29(2015).

Kocurek, G., Ewing, R.C., Mohrig, D., 2010. How do bedform patterns arise? New views on the role of bedform interactions within a set of boundary conditions. Earth Surf. Proc. Land. 35: 51-63.

Kocurek, G., Ewing, R.C., 2005. Aeolian dunefield self-organization – implications for the formation of simple versus complex dune-field patterns. Geomorphology 72: 94-105

Leibe B., A. Leonardis, and B. Schiele. Robust object detection with interleaved categorization and segmentation. International Journal of Computer Vision, 77:259–289, 2008

Li M., Zang S. Zhang B. Li S., Wu C. 2014. A Review of Remote Sensing Image Classification Techniques: the Role of Spatio-contextual Information. European Journal of Remote Sensing - 2014, 47: 389-411

Livingstone, I., Wiggs, G.F.S., Weaver, C.M., 2007. Quantifying controls on aeolian dune processes and dynamics: a review of current understanding. Earth-Sci. Rev. 80: 239-257.

Loizeau D., Poulet F., Horgan B., Mangold N., Michalski J., Bishop J. 2015. Mawrth Vallis clay unit: probing the early Mars Habitability, Climate and Origin of Life. 2nd Landing Site Workshop for the 2020 Mars Rover mission.

Matas J., O. Chum, M. Urban, and T. Pajdla. 2002. "Robust wide baseline stereo from maximally stable extremal regions." Proc. of British Machine Vision Conference, 384-396.

McKee, E.D., 1979: A Study of Global Sand Seas,ed. by E.D. McKee (Prof. Pap. U.S. Geol. Surv,Washington,D.C), 1052,p. 1

Mitasova, H., Overton, M., Harmon, R.S., 2005. Geospatial analysis of a coastal sand dunefield evolution: Jockey's Ridge, North Carolina. Geomorphology 72: 204-221

Pal. R., Pal. K., 1993. A review on image segmentation techniques. Pattern Recognition, 26 (9) (1993), pp. 1277–1294

Richards, J.A. and Jia, X., 2006, Remote Sensing Digital Image Analysis: an Introduction. Springer, Berlin, 439 p.

Silvestro, S., Fenton, L.K., Vaz, D.A., Bridges, N.T., Ori, G.G., 2010. Ripple migration and dune activity on Mars: Evidence for dynamic wind processes. Geophys. Res. Lett.

Sivaramakrishnan. A, Karnan M., Sivakumar R., 2014. Medical Image Analysis – A Review. (IJCSIT) International Journal of Computer Science and Information Technologies, Vol. 5 (1), 2014, 236-246

Soh L. and C. Tsatsoulis, 1999. Texture Analysis of SAR Sea Ice Imagery Using Gray Level Co-Occurrence Matrices, IEEE Transactions on Geoscience and Remote Sensing, vol. 37, no. 2.

Tsoar, H., Blumberg, D.G., 2002. Formation of parabolic dunes from barchan and transverse dunes along Israel's Mediterranean coast. Earth Surf. Proc. Land. 27: 1147-1161

Tsoar, H., 2001. Types of Aeolian Sand Dunes and Their Formation. Geomorphological Fluid Mechanics. N.J. Balmforth and A. Provenzale (Eds.): LNP 582, pp. 403–429, 2001. c Springer-Verlag Berlin Heidelberg

Wasson, R.J., Hyde, R., 1983. Factors determining desert dune type. Nature 304: 337-339.

Wilkins, D.E., Ford, R.L., 2007. Nearest neighbour methods applied to dunefield organization: the Coral Pink Sand Dunes, Kane County, Utah, USA. Geomorphology 83: 48-57.

Wilkinson, G.G., 1999, Recent developments in remote sensing technology and the importance of computer vision analysis techniques. Machine Vision and Advanced Image Processing in Remote Sensing vol. 1., Springer, p. 5–11
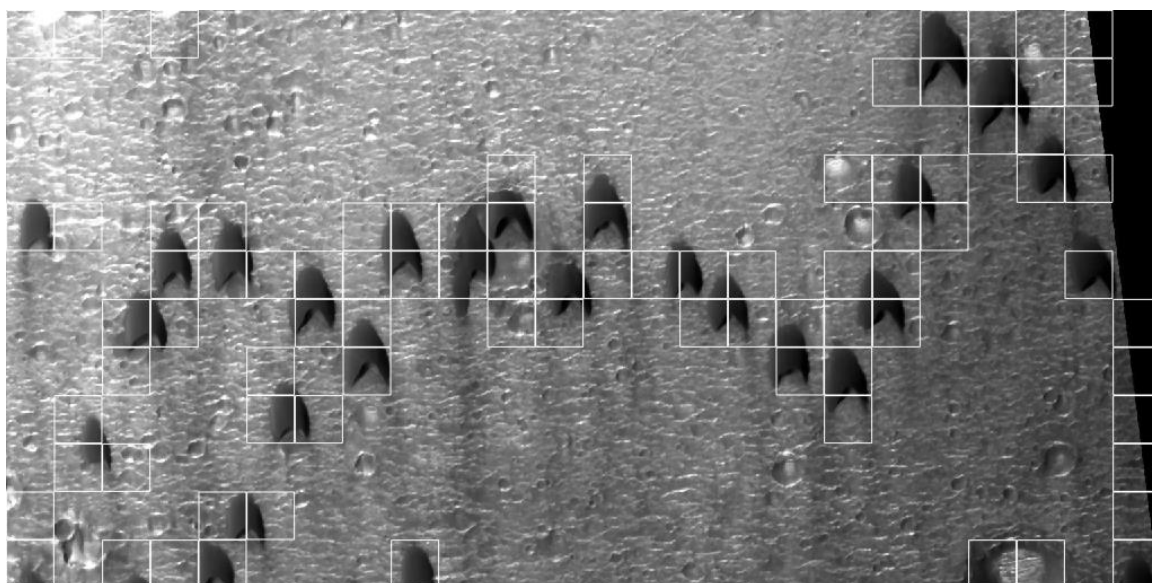
APPENDIX

The 6 following figures are representing respectively the steps
of the process of barchans detection:
(a) The result of image enhancement.
(b) The result of textural segmentation.
(c) The result of SURF features SVM classification.
(d) The result of MSER regions extraction.
(e) The result of candidate selection using [Alg.1].
(f) The HiRISE image: ESP_034815_2035, by the courtesy of
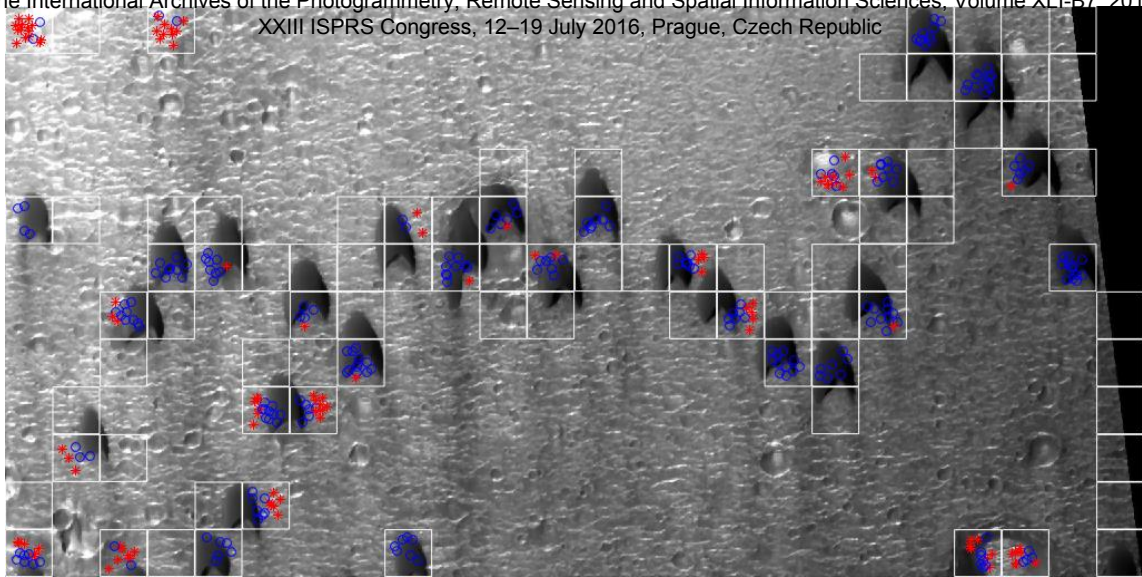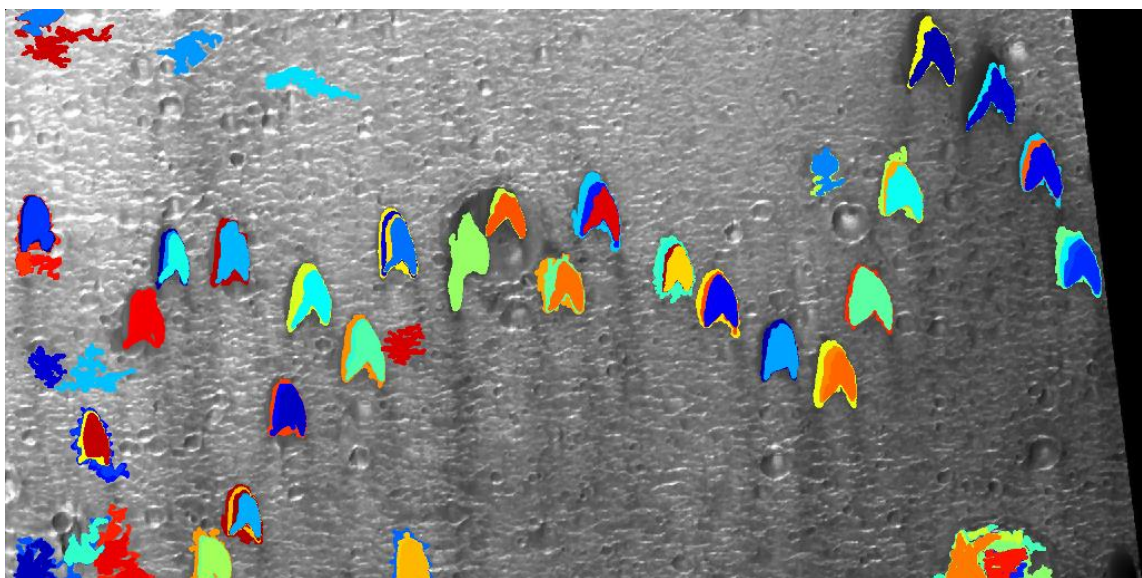NASA/JPL/University of Arizona.

(a)

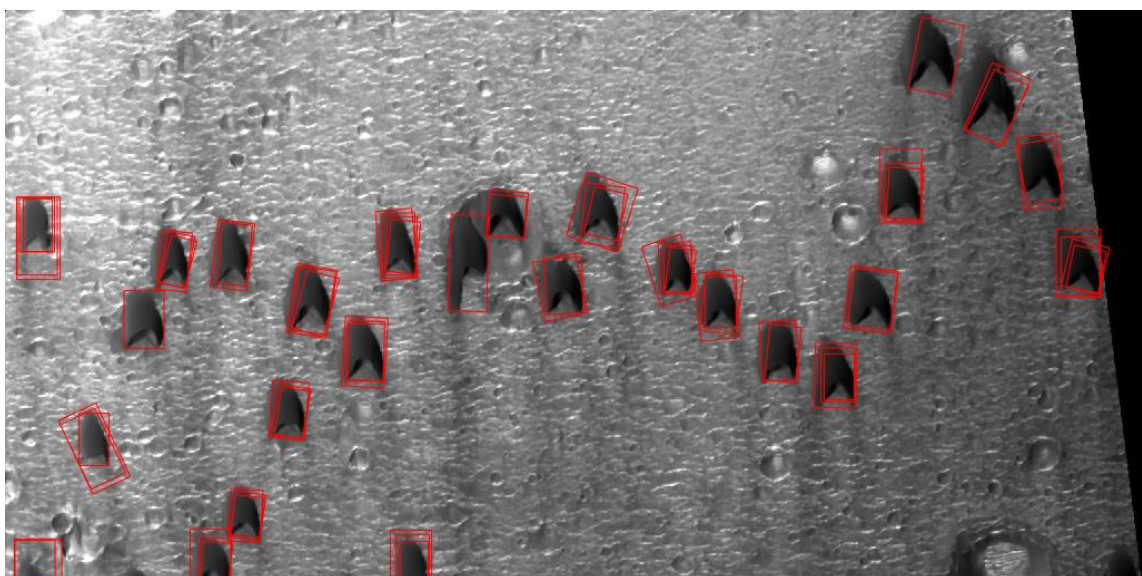(b)

(c)

(d)

(e)

(f)